

Role of cascade and Auger effects in the enhanced population of the $C^{3+}(1s2s2p^4P)$ states following single-electron capture in $C^{4+}(1s2s^3S)$ -He collisions

D. Röhrbein*

Institut für Theoretische Physik, Technische Universität Clausthal, D-38678 Clausthal-Zellerfeld, Germany

T. Kirchner†

Department of Physics and Astronomy, York University, Toronto, Ontario M3J 1P3, Canada

S. Fritzsche

*GSI Helmholtzzentrum für Schwerionenforschung, D-64291 Darmstadt, Germany and
Department of Physics, Post Office Box 3000, University of Oulu, FIN-90014 Oulu, Finland*

(Received 12 January 2010; published 5 April 2010)

The population of excited three-electron states in carbon ions after single-electron capture in 0.5–1.1 MeV/amu $C^{4+}(1s2s^3S)$ -He collisions is analyzed theoretically by combining different methods. While the two-center basis generator method is used to calculate capture amplitudes on the single-particle level, all-electron structure calculations for the relevant C^{3+} states and their radiative and Auger transition rates are performed on the multiconfiguration Dirac-Fock level. These data are then combined and fed into a set of classical rate equations for the decay dynamics. Total cross sections for the production of the $1s2s2p^4P$, $1s2s2p^2P_-$, and $1s2s2p^2P_+$ states are calculated and their ratios compared with recent experimental data and previous calculations [D. Strohschein *et al.*, Phys. Rev. A **77**, 022706 (2008)]. It is found that the relative intensities of the $1s2s2p^4P$ states are considerably larger than expected on the basis of pure spin statistics. The Auger transitions, which were not included in the previous calculations, have a significant effect on the final results in that they reduce the $1s2s2p^2P$ intensities. Although our extended computations explain a significant part of the production of the $1s2s2p^4P$ states, the experimentally observed enhancement of these states is still considerably larger than the theoretical one.

DOI: [10.1103/PhysRevA.81.042701](https://doi.org/10.1103/PhysRevA.81.042701)

PACS number(s): 34.70.+e, 34.50.Fa, 32.70.Fw, 32.80.Hd

I. INTRODUCTION

Single-electron transfer in ion-atom collisions is in general well understood. This is particularly true if the electron is captured by a bare projectile ion such that a pure one-electron state is formed. If the projectile is not bare, but carries electrons into the collision, the situation becomes more involved. One might expect that similarly configured final states which correspond to different angular momentum eigenvalues are populated according to the rules of spin statistics if the initial projectile electrons do not undergo additional transitions. However, experimental data obtained from zero-degree Auger projectile electron spectroscopy indicate that this might not be true.

Some time ago, it was recognized that capture into F^{7+} ions results in a rather strong population of the metastable $1s2s2p^4P$ final states when compared to the similarly configured $1s(2s2p^3P)^2P_-$ and $1s(2s2p^1P)^2P_+$ states [1,2]. The possible role of cascade effects was mentioned [1] but not analyzed in further detail. Recently, this enhancement of the $1s2s2p^4P$ states was determined more quantitatively for 1.1 MeV/amu $F^{7+}(1s2s^3S)$ impact on He and Ne [3]. For the case of He it was found that the measured ratio

$R = {}^4P/({}^2P_- + {}^2P_+)$ was 2.9,¹ which has to be compared to the value of 2 expected from spin statistics [4–6].

In Ref. [3] it was suggested that a dynamical Pauli exchange mechanism might be responsible for the enhancement, but it was not possible to corroborate this interpretation by theoretical calculations at that time. Zouros *et al.*, by contrast, argued that a selective cascade feeding mechanism following transfer into highly excited states causes the preferential population of the $1s2s2p^4P$ states [7,8]. They backed their interpretation by theoretical cascade calculations for F^{7+} impact on He and H_2 and obtained good agreement with the former measurements of Refs. [1,2] above 0.7 MeV/amu.

In order to shed more light on the situation, new measurements were performed for 0.5–1.0 MeV/amu $C^{4,5+}$ ions colliding with He and Ne atoms [9]. In contrast to the previous experiments, both ground-state $C^{4+}(1s^2^1S)$ and mixed-state $C^{4+}(1s^2^1S + 1s2s^3S)$ beams were used. This allowed for a more reliable separation of events obtained solely from the metastable beam component, to which the previous interpretations referred. These measurements gave rise to a ratio $R \sim 6$ –8, which is an even more pronounced departure from the spin statistics value of 2 than in the previous experiments. The effect of cascades on the

*Present address: Max-Planck-Institut für Sonnensystemforschung, D-37191 Katlenburg-Lindau, Germany.

†tomk@yorku.ca

¹ $R = {}^4P/({}^2P_- + {}^2P_+)$ is used as a shorthand notation for $R = \text{Intensity}[C^{3+}(1s2s2p^4P)]/(\text{Intensity}\{C^{3+}[1s(2s2p^3P)^2P_-]\} + \text{Intensity}\{C^{3+}[1s(2s2p^1P)^2P_+]\})$.

$C^{4+}(1s2s^3S)$ -He data was also studied in Ref. [9]. In that work, a theoretical approach conceptually similar to that of Zouros *et al.* [7,8] was set up, but based on different methods for calculating electron capture probabilities, decay rates, and the cascade dynamics. It was found that only about half of the observed enhanced population of the $C^{3+}(1s2s2p^4P)$ states is due to cascade effects; that is, room was left for other effects, such as the previously suggested Pauli mechanism.

In the present work we elaborate on those calculations and include further processes in the analysis of the $1s2s2p^{2,4}P$ populations. The methods used are described in Sec. II. In Sec. III it is demonstrated that the calculated ratio $R = 4P/(^2P_- + ^2P_+)$ is further enhanced due to the consideration of Auger processes, but the increase is not enough to explain the experimental values. Some conclusions are offered in Sec. IV. Atomic units ($\hbar = m_e = e = 1$) are used unless indicated otherwise.

II. THEORY AND COMPUTATIONS

Ion-atom collisions at MeV impact energies occur at the few-attosecond time scale, whereas Auger and radiative decays take much longer times, from 10^{-15} to 10^{-7} s, in the system under study. This warrants the separation of collision and relaxation processes and suggests a separate discussion of the methods used to describe them.

A. Calculation of the electron transfer probabilities

The collision itself is addressed with the two-center basis generator method (TC-BGM) [10], which is an extension of the original (one-center) BGM introduced in Ref. [11]. Within the semiclassical approximation and the independent electron model, the time-dependent Schrödinger equation for the active electrons is solved within a basis that is dynamically adapted to the problem. It consists of sets of bound target and projectile orbitals (including appropriate electron translation factors) and a set of pseudostates, which are constructed by the repeated application of a regularized projectile potential onto the target states.

In the present work the single-particle Hamiltonian is assumed to have the form

$$\hat{h}(t) = -\frac{1}{2}\Delta - \frac{Q_T}{r} + v_{ee}^T(r) + v_{\text{eff}}^P(r_P), \quad (1)$$

where Q_T is the charge of the target nucleus ($Q_T = 2$) and v_{ee}^T represents the effective electron potential in the He ground state. It is approximated by the exchange-only version of the optimized potential method (OPM) [12]. The effective projectile potential v_{eff}^P depends on $r_P = |\mathbf{r} - \mathbf{R}(t)|$ with the classical projectile coordinate $\mathbf{R}(t) = (b, 0, vt)$ characterized by the impact parameter b and the constant velocity v . The potential v_{eff}^P is also obtained from the OPM [13] and has the asymptotic properties

$$v_{\text{eff}}^P(r_P) = \begin{cases} -6/r_P & \text{for } r_P \rightarrow 0, \\ -4/r_P & \text{for } r_P \rightarrow \infty. \end{cases} \quad (2)$$

Using this fixed potential implies that the two electrons of the helium-like ion are assumed to be passive throughout the collision. This appears reasonable due to their relatively large

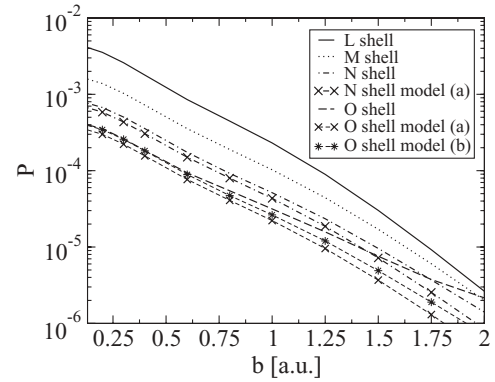


FIG. 1. Single-particle probabilities for capture into the L , M , N , and O shells for C^{4+} -He collisions at $E = 1$ MeV/amu as functions of the impact parameter. The lines without symbols represent the results of the full TC-BGM calculation. The probabilities for models (a) and (b) are obtained from an extrapolation of the results according to the $1/n^3$ scaling law when the computations were performed only up to the M shell and N shell, respectively.

binding energies and was verified by test calculations with “unfrozen” $2s$ electrons, for which the final results for $R = 4P/(^2P_- + ^2P_+)$ did not change significantly. Therefore, only the initial target electrons are propagated in order to obtain the transfer amplitudes as the main ingredients of the further analysis.

For the target basis set we use 20 states (all spatial orbitals from $1s$ to $4f_{|3|}$) and for the projectile 35 states (from $1s$ to $5g_{|4|}$) to allow for capture into (highly) excited states.² To account for the coupling to the continuum, 51 pseudostates are included in addition, so that in total the TC-BGM basis consists of 106 states. Four projectile energies ($E = 0.5, 0.75, 1$, and 1.1 MeV/amu) are considered, each with 15 impact parameters in the range $0.13 \leq b \leq 3$ a.u. The propagation started at $z = vt_0 = -45$ a.u. and ended at $z = vt_1 = +45$ a.u.

Figure 1 displays the single-particle probabilities for capture into the L , M , N , and O shells at $E = 1$ MeV/amu. Apparently, the probabilities decrease with ascending principal quantum number n . To understand to which extent they follow the well-known $1/n^3$ scaling law, we have used our results for the capture into the M and N shells to predict the capture into higher shells. More specifically, M -shell capture was used to predict capture into the N and O shells [model(a)], and N -shell capture was used to predict capture into the O shell [model(b)].³ The results show that the scaling is approximately fulfilled, except for relatively large impact parameters, where the probabilities are so small that our TC-BGM calculations become inaccurate. We have also found that the scaling is better fulfilled at higher impact energies than at the lower end of the considered interval. This is not surprising given that the scaling law is based on perturbation theory [14].

²The mirror symmetry with respect to the scattering plane is exploited such that only states with quantum numbers $nl|m|$ have to be taken into account.

³By using $P_{n+k} = \left(\frac{n}{n+k}\right)^3 P_n$.

B. Calculation of the three-electron projectile states and their decay rates

Our aim is to model and analyze the populations of the $2,4P$ levels after the collision of metastable $C^{4+}(1s2s^3S)$ projectiles with helium. Apart from the (single-electron) transfer amplitudes into the various excited shells of the projectile, this requires detailed knowledge about the formation of the three-electron states due to the capture of an electron as well as about the de-excitation of these states toward the $1s2s2p^{2,4}P$ terms. The coupling of the transferred electron to the $1s2s^3S$ term and the initial population of the various excited levels is explained in Sec. II C. Here, we describe the rates with which excited levels decay either by (Auger) electron or photon emission. These rates are uniquely determined for each level with given (total) angular momentum J and parity P while their population also depends on the magnetic (sub)states and, thus, on the magnetic quantum number M_J . Of course, only the de-excitation of the excited three-electron levels by fluorescence photons eventually leads to the $2,4P$ states of interest.

Three approximations were considered to model the populations of the excited states by capturing the transfer electron in nl subshells with either $n \leq 3, 4$, or 5 , respectively. For the metastable $1s2s^3S$ term, this gives rise to a total of 29, 55, or even 89 levels which are initially populated by the transfer process. The multiconfiguration Dirac-Fock (MCDF) method [15] has been utilized to describe the decay of these levels, based on the RATIP program [16]. Not much needs to be said about this method, which has been utilized in a larger number of case studies on the level structure and decay of atoms and ions [17]. For the photon emission, all electric-dipole ($E1$) as well as magnetic-dipole ($M1$) and electric-quadrupole ($E2$) transitions were taken into account, although only the $E1$ rates are found important for the cascade analysis. In the computation of the transition probabilities, moreover, two different gauges (Babushkin and Coulomb) were used for the coupling of the radiation field which, in the nonrelativistic limit, refer to the well-known length and velocity gauge, respectively (see Ref. [18] for details).

In contrast, the calculation of the Auger rates requires the coupling of the bound-state electrons of some excited level to the electron continuum. This coupling is caused by the interaction among the electrons but can also be affected by configuration mixing between different autoionization channels—the so-called interchannel interactions. Apart from very few case studies on the $K-LL$ and $K-LM$ spectra of noble gases, however, it has become common practice to neglect both the interchannel interactions as well as any nonorthogonality of the one-electron orbital functions in the evaluation of the Auger amplitudes. For light and medium elements, it is therefore sufficient to include the instantaneous Coulomb repulsion among the electrons. This treatment has also been implemented in the AUGER component of the RATIP program [16], in which the continuum spinors are calculated within a spherical but level-dependent potential of the final ion [19]. Both the Auger as well as the radiative rates from above are the input for the subsequent cascade analysis, which we discuss in the next section.

C. Calculation of the three-electron populations prior to the de-excitation processes and solution of the rate equations

In addition to the radiative and Auger rates discussed in Sec. II B, we need the populations of the relevant three-electron projectile states just after the collision to set up the initial conditions for the cascade dynamics. The corresponding state-to-state transition amplitudes

$$A_{if} = \langle \Phi_f | \Psi_i(t_1) \rangle \quad (3)$$

are the overlaps between the three-electron projectile states $|\Phi_f\rangle$ (calculated on the MCDF level) and the propagated states $|\Psi_i(t_1)\rangle$. The latter are antisymmetrized products of the $C^{4+}(1s2s^3S)$ states and a spin-orbital $|\psi(t_1)\rangle$ obtained from the TC-BGM propagation from t_0 to t_1 :

$$|\Psi_i(t_1)\rangle = \frac{1}{\sqrt{3}} \left(\hat{1} - \sum_{j=2}^3 \hat{P}_{1j} \right) |\psi(1, t_1)\rangle |1s2s^3S(2, 3)\rangle, \quad (4)$$

where \hat{P}_{kj} denotes a permutation operator. This construction involves again the assumption that the two projectile electrons do not undergo any transition in the course of the transfer process but remain frozen in their initial configuration. The overlaps of Eq. (3) are calculated by expanding both the propagated and final three-electron states in Slater determinants $|K^-\rangle$ such that

$$A_{if} = \langle \Phi_f | \Psi_i(t_1) \rangle = \sum_N \sum_K a_N^f d_K^i \langle N^- | K^- \rangle \quad (5)$$

with

$$\langle N^- | K^- \rangle = \det(\langle f_i | \psi_j \rangle). \quad (6)$$

The single-particle matrix elements on the right-hand side of Eq. (6) are equal to 0 or 1 if $|\psi_j\rangle$ is a frozen $1s$ or $2s$ projectile state and equal to the TC-BGM single-particle capture amplitudes if $|\psi_j\rangle$ is the propagated orbital with the same spin projection as the final-state orbital $|f_i\rangle$.

The initial conditions for the cascade analysis are obtained from averaging the state-to-state probabilities $|A_{if}|^2$ over the ensemble of equivalent initial states [of which there are six in the present case due to the coupling of one electron with two spin projections to the $C^{4+}(1s2s^3S)$ state; see Eq. (4)] and by adding up the contributions to a given fine structure level characterized by total angular momentum J and parity P ,

$$P_{J^P} = \frac{1}{6} \sum_{i, M_{J_f}} |A_{if}|^2. \quad (7)$$

For the sake of simplicity we label these populations by P_k , $k = 1, \dots, m$, in the following analysis of the cascade contributions. The standard rate equations [20,21]

$$\frac{dP_k}{dt} = \sum_{i=k+1}^m P_i(t) D_{ik}^{\text{rad}} - P_k(t) \sum_{f=1}^{k-1} D_{kf}^{\text{rad}} - P_k(t) D_{k0}^{\text{Auger}}, \quad (8)$$

$$k = 1, \dots, m,$$

are propagated numerically from times t_1 to $t_2 \sim 10^{10}$ a.u. to study the decay dynamics of the projectile ion. In Eq. (8), D_{k0}^{Auger} is the Auger (loss) rate from some upper level with label k to the (two-electron) ground state, while D_{ik}^{rad} denotes

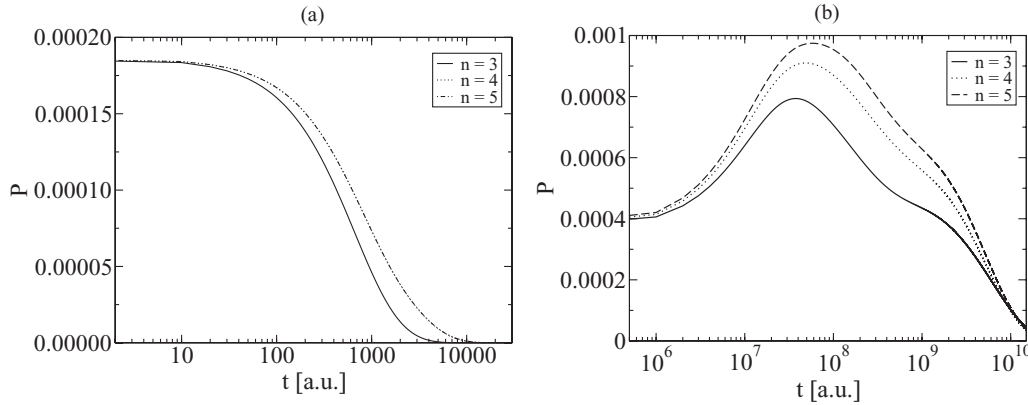


FIG. 2. Level populations of (a) the sum of $C^{3+}(1s2s2p^2P_-)$ and $C^{3+}(1s2s2p^2P_+)$ and (b) $C^{3+}(1s2s2p^4P)$ after single capture in $C^{4+}(1s2s^3S)$ -He collisions at $E = 1$ MeV/amu and $b = 0.3$ a.u. Both Auger and radiative (in length gauge) decays are included. The $n = 3$, $n = 4$, and $n = 5$ calculations are explained in the text.

the radiative transition rate between the levels i and k . As mentioned above we have checked that it suffices to include the $E1$ transitions, since the $E2$ and $M1$ rates are negligibly small.

Figure 2 shows examples of the computed time dependencies of the $1s2s2p^2P$ and $1s2s2p^4P$ levels. At $t = t_1$, the population of the quartet states is indeed twice as large as the population of the doublets, which reflects the spin statistics for direct transitions. Three sets of results are displayed in Fig. 2 corresponding to different numbers of levels included in the cascade dynamics. The first one (denoted by $n = 3$) involves all relevant levels with single-particle principal quantum numbers $n \leq 3$ (29 levels with 106 states in total), the second one all relevant levels with $n \leq 4$ (55 levels with 234 states in total), and the third one all relevant levels with $n \leq 5$ (89 levels with 434 states in total). The doublet levels (whose summed population is shown) quickly decay and are completely depleted after $t = 10000$ a.u. due to fast Auger processes. By contrast, the $1s2s2p^4P$ levels are first filled from above quite strongly until the higher-lying states are drained and decay themselves thereafter. Not surprisingly, the interim repopulation of the 4P levels increases with the number of initial levels that are included in the cascade, but the final result is the same in all cases: the quartet states are emptied (by Auger decay) only after about 10^{10} a.u. Note that the time scale is much longer than in the case of the doublet states reflecting the metastable character of the quartets.

III. RESULTS AND DISCUSSION

In the experiment, Auger electrons from the $1s2s2p^4P$ and $1s2s2p^2P_{\pm}$ states are detected along the beam direction (i.e., at zero degrees) [9]. Assuming an isotropic Auger decay and neglecting the weak radiative decays of these states, the Auger yields are proportional to the total production cross sections (TCSs). A convenient way to calculate these TCSs consists of switching off all decay processes of the $1s2s2p^2P_{\pm}$ and $1s2s2p^4P$ states; that is, all electrons are collected that are transferred to these states either directly or via cascading processes. The accumulated probabilities

are then integrated over the impact parameter to obtain the TCSs, and the experimental ratio $R = ^4P/(^2P_- + ^2P_+)$ can be compared to the corresponding cross-section ratio.

We have calculated the radiative rates in both length and Coulomb gauges. Figure 3 compares results obtained from both gauges at $E = 1$ MeV/amu and $b = 0.3$ a.u. No gauge dependence is observed for the $1s2s2p^2P_{\pm}$ levels. If their decay rates are switched off, their populations do not change with time; that is, they are not filled from above, since the decay dynamics of the doublet states is dominated by Auger processes [cf. Fig. 2(a)]. The $1s2s2p^4P$ levels, by contrast, are filled from above, and the time development of the populations varies slightly in both gauges. However, the final populations remain almost gauge independent and are appropriate to determine the TCS.

Auger processes were not included in our previous calculations published along with the experimental data in Ref. [9]. In Fig. 4 we show for the same kinematic parameters as above how the dynamics change if this decay channel is taken into

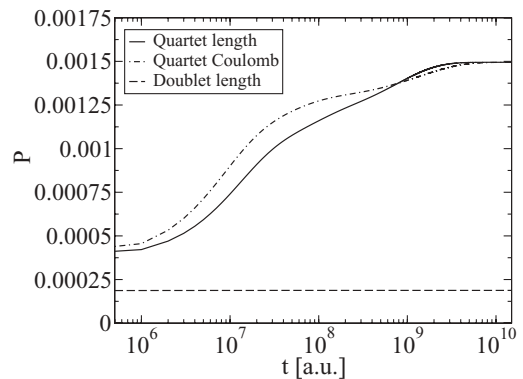


FIG. 3. Level populations of the sum of $C^{3+}(1s2s2p^2P_-)$ and $C^{3+}(1s2s2p^2P_+)$ (doublet), and $C^{3+}(1s2s2p^4P)$ (quartet) after single capture in $C^{4+}(1s2s^3S)$ -He collisions at $E = 1$ MeV/amu and $b = 0.3$ a.u. with decay processes from these states switched off (see text). For higher-lying levels (up to $n = 5$), both Auger and radiative decays (in length and Coulomb gauges) are included. In the case of the doublet states, only results obtained in length gauge are displayed. The Coulomb gauge gives indistinguishable results.

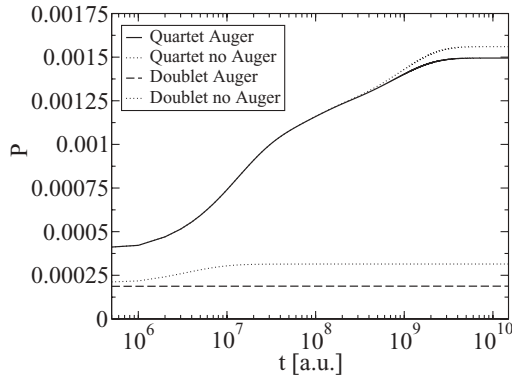


FIG. 4. Level populations of the sum of $C^{3+}(1s2s2p^2P_{-})$ and $C^{3+}(1s2s2p^2P_{+})$ (doublet), and $C^{3+}(1s2s2p^4P)$ (quartet) after single capture in $C^{4+}(1s2s^3S)$ -He collisions at $E = 1$ MeV/amu and $b = 0.3$ a.u. with decay processes from these states switched off (see text). For higher-lying levels (up to $n = 5$), the Auger decay is either included or not, while the radiative decay is always included in length gauge.

account for the higher-lying levels. Clearly, the Auger effect does play a significant role, in particular for the doublet states. If it is neglected, the $1s2s2p^2P_{\pm}$ levels are fed from above radiatively, and the denominator in the ratio R is increased. The $1s2s2p^4P$ levels are also affected by Auger processes, but the reduction of the final populations is somewhat smaller than in the case of the doublets. Consequently, the numerator in R also decreases if Auger decays are taken into account, but by a smaller amount than the denominator. The net effect is an increase of R (see later discussion).

In order to provide a more comprehensive comparison between our current and previous results, we show TCSs for the production of the $1s2s2p^4P$ and $1s2s2p^2P_{\pm}$ levels in Fig. 5. Analogously to Fig. 2, results are displayed which correspond to the inclusion of levels up to $n \leq 3$, $n \leq 4$, and $n \leq 5$ into the cascade analysis in order to demonstrate the convergence behavior with respect to the number of excited three-electron states. If Auger processes are forbidden, the TCSs are generally larger and they increase with increasing number of excited states. For the quartet states, the latter tendency is also observed if Auger processes are included,

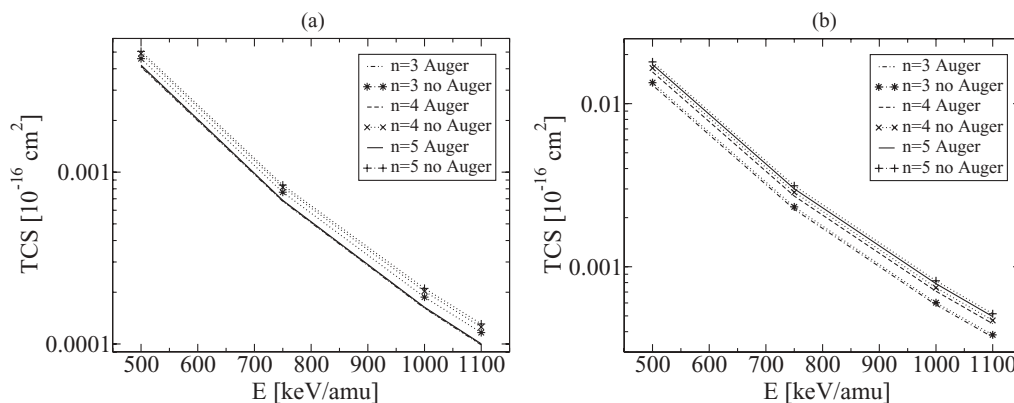


FIG. 5. TCSs for the production of (a) the sum of $C^{3+}(1s2s2p^2P_{-})$ and $C^{3+}(1s2s2p^2P_{+})$ and (b) $C^{3+}(1s2s2p^4P)$ after single capture in $C^{4+}(1s2s^3S)$ -He collisions as functions of the impact energy. For higher-lying levels, the Auger decay is either included or not, while the radiative decay is always included in length gauge. The $n = 3$, $n = 4$, and $n = 5$ calculations are explained in the text.

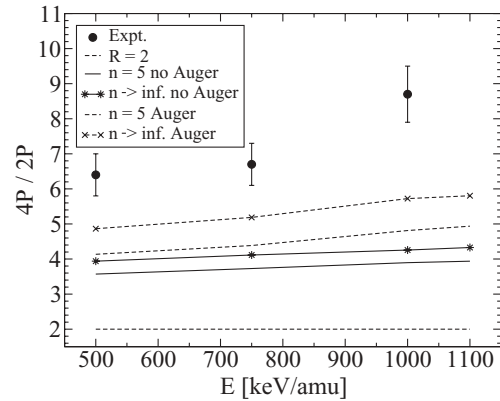


FIG. 6. Experimental [9] and theoretical ratio $R = ^4P / (^2P_{-} + ^2P_{+})$ after single capture in $C^{4+}(1s2s^3S)$ -He collisions as a function of the impact energy. Auger decays are or are not included, while radiative decays are always included in length gauge. The $n = 5$ and $n \rightarrow \infty$ calculations are explained in the text.

but the situation is different for the doublet states. Here the results are virtually identical, independent of the number of upper-lying levels that are considered in the transfer process. This confirms what was pointed out before by Zouros *et al.* [7,8]: in the case of the doublets, fast Auger processes to the $1s^2^1S$ ground state dominate and suppress radiative decays. By contrast, the latter prevail for the quartets. As a consequence, the ratio R does not reflect simple spin statistics but assumes a larger value because of a selective cascade feeding mechanism.

Finally, the ratio $R = ^4P / (^2P_{-} + ^2P_{+})$ is shown in Fig. 6. We compare the experimental ratio to our most elaborate previous (no Auger) and current (Auger) calculations, in which all states with $n \leq 5$ are included. As expected from the preceding analysis, the current calculations give somewhat larger values than the older ones. In Ref. [9] we demonstrated that R increases with increasing number of included excited states and we suggested applying the $1/n^3$ scaling to obtain an extrapolated value of R for $n \rightarrow \infty$. We have also used this procedure here and include corresponding results in Fig. 6.

One can see that our new calculations, which include Auger decays, come closer to the experimental ratio but are still well outside the error bars.

IV. CONCLUSIONS

In this paper we have extended our previous theoretical calculations for single-electron capture in $C^{4+}(1s2s^3S)$ -He collisions to account for further details of the (re)population of the projectile states due to various decay processes. Nonperturbative collision calculations, *ab initio* structure calculations, and a straightforward (numerical) analysis of the decay dynamics have been combined to probe recent experimental data obtained from zero-degree Auger projectile electron spectroscopy, according to which the $C^{3+}(1s2s2p^4P)$ levels are populated more strongly than expected from pure spin statistics compared with the 2P levels of the same configuration. Clearly, our calculations show that cascade processes contribute to this enhancement. In a previous work, in which Auger decays were not taken into account, we concluded that about half of the observed enhancement originates from

cascaes. Our present, more complete analysis suggests that approximately 70% can be attributed to the capture into higher-lying states, along with their subsequent decay dynamics. However, there is still room left for other effects. Whether this is the dynamical Pauli exchange mechanism proposed in Ref. [3] or something else is presently an open question. Unfortunately, a quantitative test of the exchange mechanism would require a very demanding collision calculation on the time-dependent Hartree-Fock level (or beyond) for the three-electron problem.

ACKNOWLEDGMENTS

T.K. acknowledges support from the Natural Sciences and Engineering Research Council of Canada and S.F. acknowledges the support from the Deutsche Forschungsgemeinschaft.

-
- [1] D. H. Lee, P. Richard, J. M. Sanders, T. J. M. Zouros, J. L. Shinpaugh, and S. L. Varghese, *Nucl. Instrum. Methods Phys. Res. B* **56**, 99 (1991).
 - [2] D. H. Lee, P. Richard, J. M. Sanders, T. J. M. Zouros, J. L. Shinpaugh, and S. L. Varghese, *Phys. Rev. A* **44**, 1636 (1991).
 - [3] J. A. Tanis, A. L. Landers, D. J. Pole, A. S. Alnaser, S. Hossain, and T. Kirchner, *Phys. Rev. Lett.* **92**, 133201 (2004).
 - [4] E. P. Benis, T. J. M. Zouros, T. W. Gorczyca, A. D. Gonzalez, and P. Richard, *Phys. Rev. A* **69**, 052718 (2004).
 - [5] E. P. Benis, T. J. M. Zouros, T. W. Gorczyca, A. D. Gonzalez, and P. Richard, *Phys. Rev. A* **73**, 029901(E) (2006).
 - [6] J. A. Tanis, A. L. Landers, D. J. Pole, A. S. Alnaser, S. Hossain, and T. Kirchner, *Phys. Rev. Lett.* **96**, 019901(E) (2006).
 - [7] T. J. M. Zouros, B. Sulik, L. Gulyás, and K. Tökési, *Phys. Rev. A* **77**, 050701(R) (2008).
 - [8] T. J. M. Zouros, B. Sulik, L. Gulyás, and K. Tökési, *J. Phys. Conf. Ser.* **163**, 012004 (2009).
 - [9] D. Strohschein, D. Röhrbein, T. Kirchner, S. Fritzsche, J. Baran, and J. A. Tanis, *Phys. Rev. A* **77**, 022706 (2008).
 - [10] M. Zapukhlyak, T. Kirchner, H. J. Lüdde, S. Knoop, R. Morgenstern, and R. Hoekstra, *J. Phys. B* **38**, 2353 (2005).
 - [11] O. J. Kroneisen, H. J. Lüdde, T. Kirchner, and R. M. Dreizler, *J. Phys. A* **32**, 2141 (1999).
 - [12] E. Engel and S. H. Vosko, *Phys. Rev. A* **47**, 2800 (1993).
 - [13] E. Engel (private communication).
 - [14] K. Omidvar, *Phys. Rev.* **153**, 121 (1967).
 - [15] I. P. Grant, in *Methods in Computational Chemistry*, edited by S. Wilson (Plenum, New York, 1989), Vol. 2, p. 1.
 - [16] S. Fritzsche, *J. Electron Spectrosc. Relat. Phenom.* **114**, 1155 (2001).
 - [17] S. Fritzsche, *Phys. Scr.* **T100**, 37 (2002).
 - [18] C. Z. Dong, S. Fritzsche, B. Fricke, and W.-D. Sepp, *Mon. Notes Astron. Soc.* **307**, 809 (1999).
 - [19] S. Fritzsche, B. Fricke, and W.-D. Sepp, *Phys. Rev. A* **45**, 1465 (1992).
 - [20] L. J. Curtis, *Am. J. Phys.* **36**, 1123 (1968).
 - [21] S. M. Younger and W. L. Wiese, *Phys. Rev. A* **17**, 1944 (1978).